

Supporting Information for

Single-charge transport through hybrid core-shell Au-ZnS quantum dot: A comprehensive analysis from the modified energy structure

Tuhin Shuvra Basu,^{a,b*} Simon Diesch,^a Ryoma Hayakawa,^b Yutuka Wakayama,^b Elke Scheer^a

^aDepartment of Physics, University of Konstanz, 78457 Konstanz, Germany. ^bInternational Center for Materials Nanoarchitectonics (WPI-MANA), National Institute for Materials Science (NIMS), 1-1 Namiki, Tsukuba, Ibaraki 305-0044, Japan.

A. Detailed fabrication route of hybrid core-shell Au-ZnS quantum dots (QDs)

All the chemicals are procured commercially and, except for the solvents, are used as purchased. Dry solvents are obtained through a solvent purification system with an extremely low ppm (<20 ppm) level of oxygen and moisture. The whole process is carried out in a glovebox under inert N₂ atmosphere. The multistep process has been described in the following section.

i. Growth of the monodisperse oleylamine capped Au nanocrystals (NCs): The synthesis method is based on the controlled nucleation of the metallic core by injection of AuCl₃ in hot oleylamine. Oleylamine can precisely control the diameter of the NCs.¹ In a typical synthesis, 0.04 g (or 12 mM) of AuCl₃ is dissolved in 10 mL of oleylamine by 10 min sonication. This reaction mixture forms Au-oleate complexes with an orange colour. The mixture is then heated, stirred, and maintained at 100°C for ~30 min. During this time, the color of the reaction mixture changed from orange to deep purple (Fig. 1a of main text). The solution is cooled to room temperature and is transferred to centrifuge tubes. After cleaning by successive centrifugation with dry methanol, the supernatant is dissolved in 5 mL toluene.

ii. Core-shell bi-metallic Au-Ag core-shell NCs: In this step Au NCs from the previous step are dissolved in 5 mL of oleylamine (1:1). The temperature of the Au NC/oleylamine solution is raised to and maintained at 120°C while stirring to evaporate the toluene. Then, a 12 mM solution of AgNO₃ (in deionized water) is prepared to keep the parity of the Au NC ensemble. Initially 0.2 mL AgNO₃ is added to the flask dropwise and the reaction temperature is kept at 120°C with continuous stirring for 10 min. The AgNO₃ has been reduced in the presence of oleylamine and then Ag grew on the top of the Au NCs due to thermodynamically favourable conditions. After 10 min we take out the solvent from the flask for absorption measurement by UV-Vis spectroscopy. We stepwise add AgNO₃ and monitor the blue shift in the LSPR peak. The concentration of Ag is controlled so that there is no change in the formation of isolated Ag NC. After the desired LSPR peak shift is attained, the reaction solution is cooled to room temperature. Excess dry methanol is added to the solution and is successively centrifuged for cleaning. The precipitate is then suspended in toluene.

iii. Formation of core-shell Au-Ag₂S NCs: This step is vital for the final hybrid metal-semiconductor core-shell Au-ZnS QDs. The electronegativity of Ag is similar those of chalcogenides like ZnS. Under certain conditions (e.g. appropriate

temperature and anion molecular complexes), the silver shells in stage (ii) can be modified to form Ag compound shells (Ag_2S) with an amorphous structure, providing a crucial platform for the next monocrystalline growth. The Au-Ag NCs from the previous procedure is mixed with 0.2 mL of S precursor with 3 mM. The solvent has been stirred vigorously and then left to react for 10 min. After 10 min, a sample is taken for spectral analysis. The NCs are then again cleaned by adding dry methanol to the reaction solution and centrifuging the solution repeatedly for at least 3-4 times. Under N_2 , the precipitated Au- Ag_2S NCs are then suspended in toluene.

iv. Hybrid metal-semiconductor core-shell Au-ZnS QDs: Finally, 0.01 g of $\text{Zn}(\text{NO}_3)_2$ is added to 5 mL of dry methanol and sonicated for 20 min. Separately, the Au/ Ag_2S NCs from the previous step in the synthesis is injected under N_2 . After sonication, the $\text{Zn}(\text{NO}_3)_2$ solution and 0.1 mL of tri-butyl phosphine (TBP) are injected, and temperature has been maintained at, 50-60°C for 120 min under vigorous stirring under N_2 . TBP is selected because it is a soft base and can behave as a phase-transfer agent to transport Zn-ions to the surface of the core NCs by binding to free cations. The high acid softness of Ag^+ favours the exchange process between Ag^+ in the amorphous matrix and Zn^{2+} in solution. During the substitution, the colour of the solvent changes first to dark blue and then to nearly transparent blue (Fig. 2a of the main text). The contents are then cooled to room temperature. Dry methanol is added to the reaction mixture, which is subsequently centrifuged for cleaning and finally dispersed in toluene.

B. HR-TEM of Au NCs

Fig. S1 shows a HR-TEM image of the Au NCs showing the narrow size distribution.

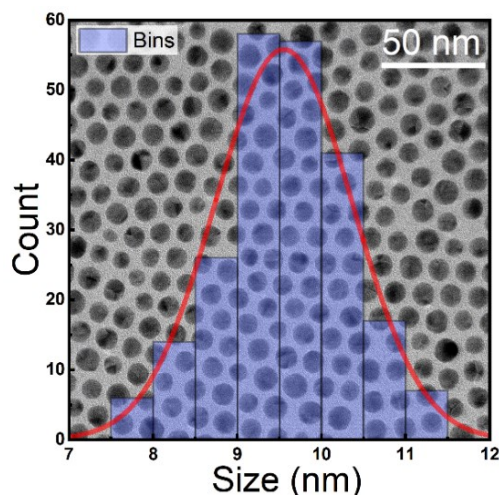


Fig. S1 HR-TEM image represents the nearly monodisperse Au NCs. Histogram shows a mean diameter of 9.5 nm of the Au NCs. Blue columns represent the number of particles with specific size and red line is the normal distribution curve based on the bins.

The size of the Au NCs mostly varies between 9-10 nm. The histogram of the entire micrograph has a normal distribution with a mean diameter of 9.5 nm with variance (σ^2) = 0.66. Most of the Au NCs we coat with Ag nano shells have a diameter of 9 nm (see main text).

C. HR-TEM of bimetallic core-shell Au-Ag NCs

Fig. S2 represents the HR-TEM image of Au-Ag NCs.

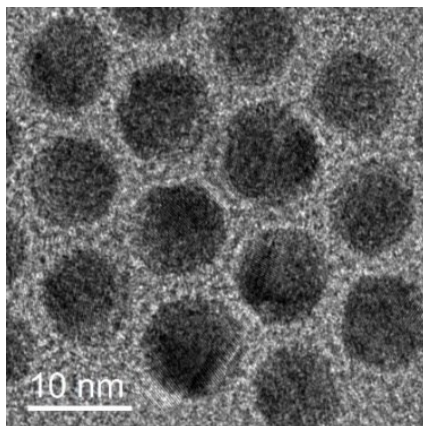


Fig. S2 HR-TEM image presents the distribution of Au-Ag NCs with most of the particles having diameters of 12 nm. We collect the aliquot of Au-Ag NCs (in toluene) to see the dispersity of the NCs in HR-TEM. The micrograph shows that all the NCs have a diameter of 12 nm. We did not show any histogram as the number of particles we are showing is limited.

D. Preparation of samples with Si NCs for STM

The STM has a scanning area of about ($1 \mu\text{m} \times 1 \mu\text{m}$).² In the present study, the scanning area has been kept as small as ($50 \text{ nm} \times 50 \text{ nm}$) due to limited scan speed to locate QDs.^{3,4} We use an atomically flat Au film deposited on mica obtained from PHASIS Sàrl, Switzerland. To increase the probability of having the QDs inside the low scanning area we deposit a monolayer of 1,6-hexanedithiol (HDT) on the top of the Au-film. First, we thermally anneal the Au-film by a butane blow torch keeping the temperature at 300°C for $\sim 10\text{s}$. Then a self-assembled monolayer (SAM) is grown by HDT dissolved in 2 mM methanol solution by immersing Au film inside the solvent for 40 min inside a glovebox. Then the substrate has been cleaned by methanol and dried by a N_2 flow. One thiol group has been attached to the Au film and another thiol group end is open. Then the dithiol treated Au films have been immersed in solutions containing Au NCs, Au-Ag NCs, Au-Ag₂S NCs or Au-ZnS QDs for ~ 45 min inside a glovebox. All the NCs and QDs easily to the thiol group physisorption or chemisorption. The samples are then annealed indirectly at 60°C for 12 min on a hot plate to evaporate the excess solvent. We transfer the prepared substrates to the STM chamber and immediately pump to moderate vacuum (10^{-4} mbar) before we cool down within ~ 2 hours to cryogenic vacuum conditions.²

E. Set-up parameters during STM imaging and STS

We perform STM imaging and STS with a UNISOKU Pt-Ir tip (apex radius 10 nm) in a custom-made STM mounted in a ^3He cryostat at 300 mK. The set-up was built and refined by previous group members.²⁻⁵ The STM controller is a

commercially available R9 system by RHK Technology with special low-noise current amplifier (IVP-100 and IVP-300). We scan slowly in the x-direction to achieve low-noise topography images with (512×512) data points. The topography images are achieved in a constant current mode with the STM feedback loop set to a tunnelling current of 100-150 pA at 1.0-1.5 V bias voltage. The I-V curves in the tunnelling regime are recorded by positioning the STM tip above an individual QD. During STS, the feedback loop was switched off. The bias voltage is then modulated with an ac voltage, with a 40-mV r.m.s. amplitude and frequency 733 Hz for recording dI/dV spectra via a lock-in technique. We used a current-to-voltage converter with 1 V nA^{-1} gain, and the measuring time is 30 s per spectrum. The tunnel resistance has been varied from 1-5 $\text{G}\Omega$ to have a good stability of the tip and to keep a safe distance between tip and QDs during data acquisition. The dI/dV spectra are obtained by averaging subsequent repetitive voltage sweeps. Single electron tunnelling (SET) can be clearly observed as the total tunnelling resistance (R_T) is much larger (\sim few $\text{G}\Omega$) than the quantum resistance $h/e^2 = 25.8 \text{ k}\Omega$. Thermal energy smearing ($k_B T$) at 300 mK is 0.026 meV and is much lower than the charging energy $\Sigma(r)$ of a typical QD (0.04 eV).

F. I-V characteristics of Au NC, Au-Ag₂S hybrid nanostructure and Au-ZnS QD

Fig. S3 represents the I-V characteristic of Au NCs performed by STM. The I-V curve shows prominent zero-conductance-gap and Coulomb staircases other related to Au NC.

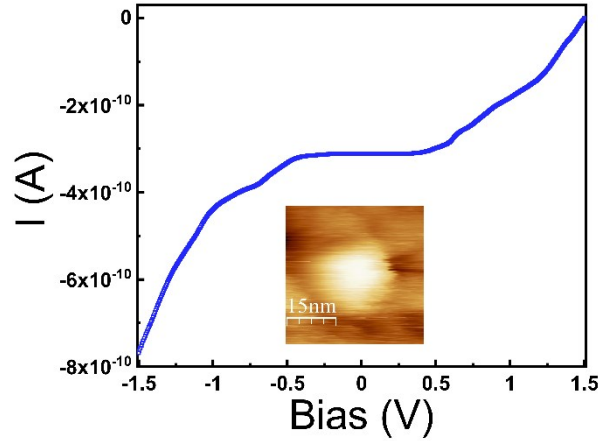


Fig. S3 I-V characteristic of Au NC measured by STM.

Fig. S2 (a) shows the I-V characteristic of Au-Ag₂S core-shell nanostructure and (b) exhibits I-V of Au-ZnS hybrid core-shell QD. Both the curves show pronounce zero-conductance-gap. But the other features related to electronic structure is not prominent as conductance curves shown in the main text.

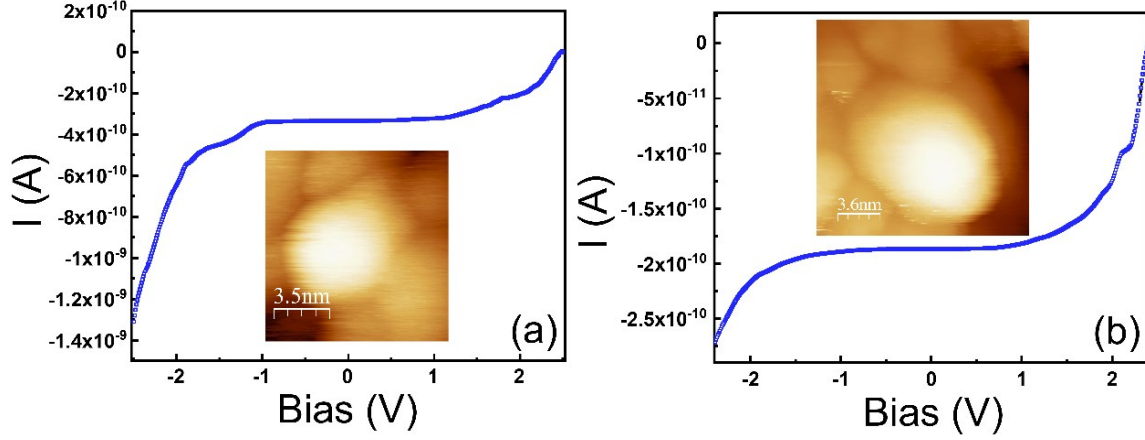


Fig. S4 I-V characteristic of (a) Au-Ag₂S core-shell hybrid nanostructure and (b) Au-ZnS QDs measured by STM.

G. Simulation of the tunnel transport characteristic by the Orthodox Theory of Au NC and Au-Ag core-shell NC

Here we provide a comparison between experiment and theory related to tunnel transport. For this type of double tunnel junction system, we can apply the Orthodox Theory to observe the tunnel characteristic of the NC. According to the Orthodox Theory, the tunnelling rate in the respective junction (termed as i^{th} junction) can be expressed as:⁶

$$\Gamma_i^{\pm}(n) = \left(\frac{1}{R_i e^2} \right) \left[\frac{-\Delta E_i^{\pm}}{1 - e^{(\Delta E_i^{\pm}/k_B T)}} \right] \quad 1$$

\pm suggests either ‘tip-to-QD system’ or ‘QD system-to-tip’ tunnelling across the junctions ($n \rightarrow n \pm 1$). ΔE_i^{\pm} represents the change in energy while the electron tunnels through the insulating layer. The tunnelling rate $\Gamma_i^{\pm}(n)$ is inversely proportional to the junction resistance. Now considering the electrostatic energy in each junction ($e > 0$), we obtain:

$$\Delta E_1^{\pm} = \left(\frac{e}{C_1 + C_2} \right) \left[\frac{e}{2} \pm (ne - Q_0) \mp C_2 V \right];$$

$$\Delta E_2^{\pm} = \left(\frac{e}{C_1 + C_2} \right) \left[\frac{e}{2} \pm (ne - Q_0) \pm C_1 V \right] \quad 2$$

Q_0 is the fractional residual charge inside the NC/QD system and $Q_0(\text{mod } e)$ can be expressed by equation^{6,7}

$$Q_0 = \frac{1}{e} [C_2(\Delta\Phi_2) - C_1(\Delta\Phi_1)] \quad 3$$

$\Delta\Phi_1$ and $\Delta\Phi_2$ are the contact potentials around junctions 1 and 2. The fractional residual charge for the metallic NC system is $\sim 0.1e$.

The collective electronic distribution on the NC is

$$\sigma(n)[\Gamma_1^+(n) + \Gamma_2^+(n)] = \sigma(n+1)[\Gamma_1^-(n+1) + \Gamma_2^-(n+1)] \quad 4$$

where $\sigma(n)$ is the ensemble distribution of the number of electrons on the central electrode. In the above expression the overall probability of electron tunnelling between two neighbouring states in steady state is zero. Combining the above equations, the tunnelling rate Γ_i^\pm can be expressed by the tunnelling current $I(V)$ with the normalization

$$\sum_{n=-\infty}^{\infty} \sigma(n) = 1$$

condition . Therefore, the tunnel current in two adjacent tunnel junctions becomes

$$I(V) = e \sum_{n=-\infty}^{\infty} n\sigma(n)[\Gamma_2^-(n) - \Gamma_2^+(n)] = e \sum_{n=-\infty}^{\infty} n\sigma(n)[\Gamma_1^+(n) - \Gamma_1^-(n)] \quad 5$$

Further, from the $I(V)$ curves, we can calculate the differential conductance curves by numerical derivation. In the present work we did the numerical analysis by a circuit simulator of single electron transport named as SOMON 2.0 (<https://www.lybrary.com/simon/>). This simulator is a Monte Carlo simulator for the rate equation. To have a precise simulation we inserted several parameters, e.g., tunnelling resistances, tunnelling capacitances, background charge, and type of the material from the experiment. The values of the capacitances are estimated from the Coulomb blockade gap (zero-conductance-gap of Fig. 2) in the main text.

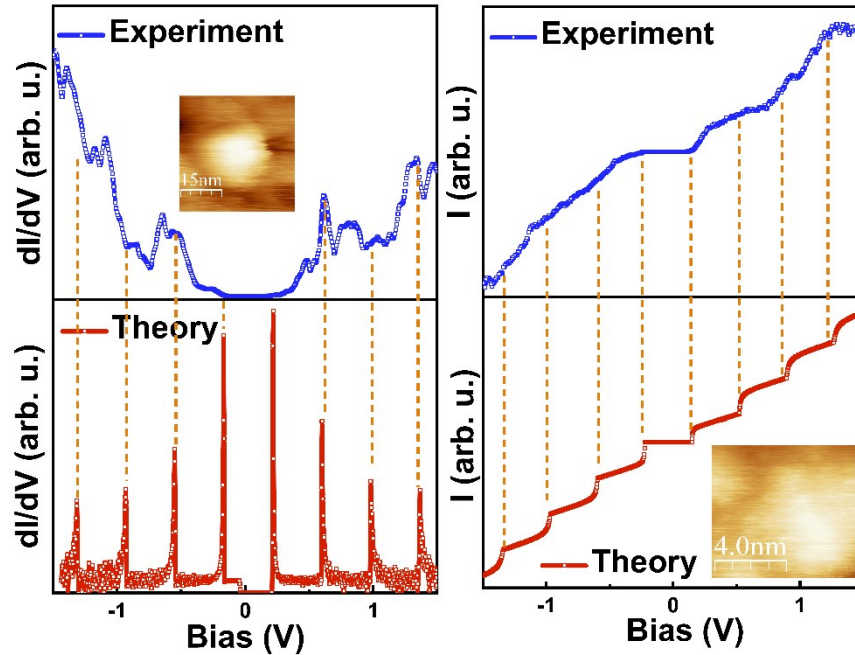


Fig. S5 and S6 show the comparison of the tunnel transport between experiment and theory of a Au NC (left) and a Au-Ag core-shell NC (right).

Unlike other tunnelling parameters we could not utilize the tunnelling resistances from the experimental curve due to nonlinearity in the I-V curves. Therefore, our approach is to match the experimental and theoretical curves by changing the resistance ratio of the two junctions, since the resistance ratio determines the profile of the curve and therefore allows us to determine this ratio. In the present case we observed that both for the Au NC and Au-Ag core-shell NC the ratio is ~ 1000 . The comparisons between simulated and experimental data for the two cases are shown in the Fig. S5 (Au NC) and Fig. S6 (Au-Ag core-shell NC). We observe exceptionally good agreement between the experiment and theory regarding the position of the steps/peaks and regarding the relative height of the staircase steps. However, there are differences concerning the step sharpness/peak heights, because in the experimental curves we also have contributions to noise which result in rounding of the features. Furthermore, the simulation model assumes a uniform island without substructure and with featureless density of states of both the island and the leads. The detailed variations in the tunnel transport due to the complex geometry cannot be predicted by the Orthodox theory in this simple form.

References

1. S. Mourdikoudis and L. M. Liz-Marzan, *Chem. Mater.*, 2013, **25**, 1465-1476.
2. C. Debuschewitz, F. Munstermann, V. Kunej and E. Scheer, *J Low Temp. Phys.*, 2007, **147**, 525-535.
3. T. S. Basu, S. Diesch and E. Scheer, *Nanoscale*, 2018, **10**, 13949-13958.

4. T. S. Basu, S. Diesch, M. Obergfell, J. Demsar and E. Scheer, *Phys. Chem. Chem. Phys.*, 2019, **21**, 13446-13452.
5. M. Wolz, C. Debuschewitz, W. Belzig and E. Scheer, *Phys. Rev. B*, 2011, **84**.
6. A. E. Hanna and M. Tinkham, *Phys. Rev. B*, 1991, **44**, 5919-5922.
7. J. G. A. Dubois, E. N. G. Verheijen, J. W. Gerritsen and H. Vankempen, *Phys. Rev. B*, 1993, **48**, 11260-11264.